CMLS, Cell. Mol. Life Sci. 58 (2001) 194–204
1420-682X/01/020194-11 $ 1.50 + 0.20/0

CMLS Cellular and Molecular Life Sciences

Structure and function of eukaryotic NAD(P)H:nitrate reductase

W. H. Campbell

Department of Biological Sciences, Phytotechnology Research Center, Michigan Technological University, Houghton (Michigan 49931, USA), Fax + 1 906 487 3167, e-mail: wcampbel@mtu.edu

Abstract. Pyridine nucleotide-dependent nitrate reductases (NRs; EC 1.6.6.1–3) are molybdenum-containing enzymes found in eukaryotic organisms which assimilate nitrate. NR is a homodimer with an ~100 kDa polypeptide which folds into stable domains housing each of the enzyme's redox cofactors—FAD, heme-Fe molybdopterin (Mo-MPT) and the electron donor NAD(P)H—and there is also a domain for the dimer interface. NR has two active sites: the nitrate-reducing Mo-containing active site and the pyridine nucleotide active site formed between the FAD and NAD(P)H domains. The major barriers to defining the mechanism of catalysis for NR are obtaining the detailed three-dimensional structures for oxidized and reduced enzyme and more in-depth analysis of electron transfer rates in holo-NR. Recombinant expression of holo-NR and its fragments, including site-directed mutagenesis of key acative site and domain interface residues, are expected to make large contributions to this effort to understand the catalytic mechanism of NR.

Key words. Nitrate reductase; pyridine nucleotides; recombinant expression; *Pichia pastoris*; site-directed mutagenesis; structure and function analysis; redox potential; *Arabidopsis*; *Zea mays*.

Introduction

The assimilatory NAD(P)H:nitrate reductases (NRs; EC 1.6.6.1–3) are a widespread family of closely related molybdenum-containing enzymes in plants, fungi and algae, which were recently reviewed in detail [1]. NR catalyzes reduction of nitrate of nitrite driven by NAD(P)H (fig. 1a) which is an irreversible reaction and a highly regulated process of nitrogen acquisition in these organisms [2]. NR is a soluble enzyme composed of an ~100-kDa polypeptide which binds 1 equivalent of molybdenum-molybdopterin (Mo-MPT), heme-Fe and FAD. Dimerization is required for activity, and the native NR is a homodimer with a tendency to further dimerize to a homotetramer (dimer of dimers), with this difference expected to make only a slight impact on functionality. NR has two active sites, which are joined by the internal electron transport pathway from FAD via heme-Fe to the Mo-MPT. In the first active site, electrons are donated to the enzyme at the FAD by NADH, or NADPH in specific isoforms or both in various bispecific isoforms of NR, with this difference in pyridine nucleotide specificity being the major functional feature distinguishing the family members. In the second active site, two electrons are transferred from the reduced Mo^{IV} to nitrate, reducing it to nitrite and hydroxide. With this physical separation of the active sites joined by the electron transfer pathway, the steady-state kinetics of NR have the best fit to a two-site ping-pong steady-state kinetic mechanism with $NAD(P)^+$ competing with NAD(P)H in a mutually exclusive manner in one active site and nitrite competing with nitrate in the same way in the other active site. Both products are weak inhibitors with millimolar K_i values, whereas K_m values for NADH and nitrate are in the low micromolar range. NR has partial activity with electron acceptors like ferricyanide (FeCN) and Cyt *c* accepting electrons directly from the FAD and heme-Fe, respectively, and with reduced dyes driving nitrate reduction directly at the Mo-MPT in the nitrate-reducing active site or via the Cyt *b* domain where heme-Fe is housed (fig. 1a). NR has a k_{cat} for NADH reduction of nitrate of 200–300 s^{-1} at 30 °C [1]. Since both sets of partial activities have greater k_{cat} values than NADH-driven nitrate reduction, it appears that internal elec-

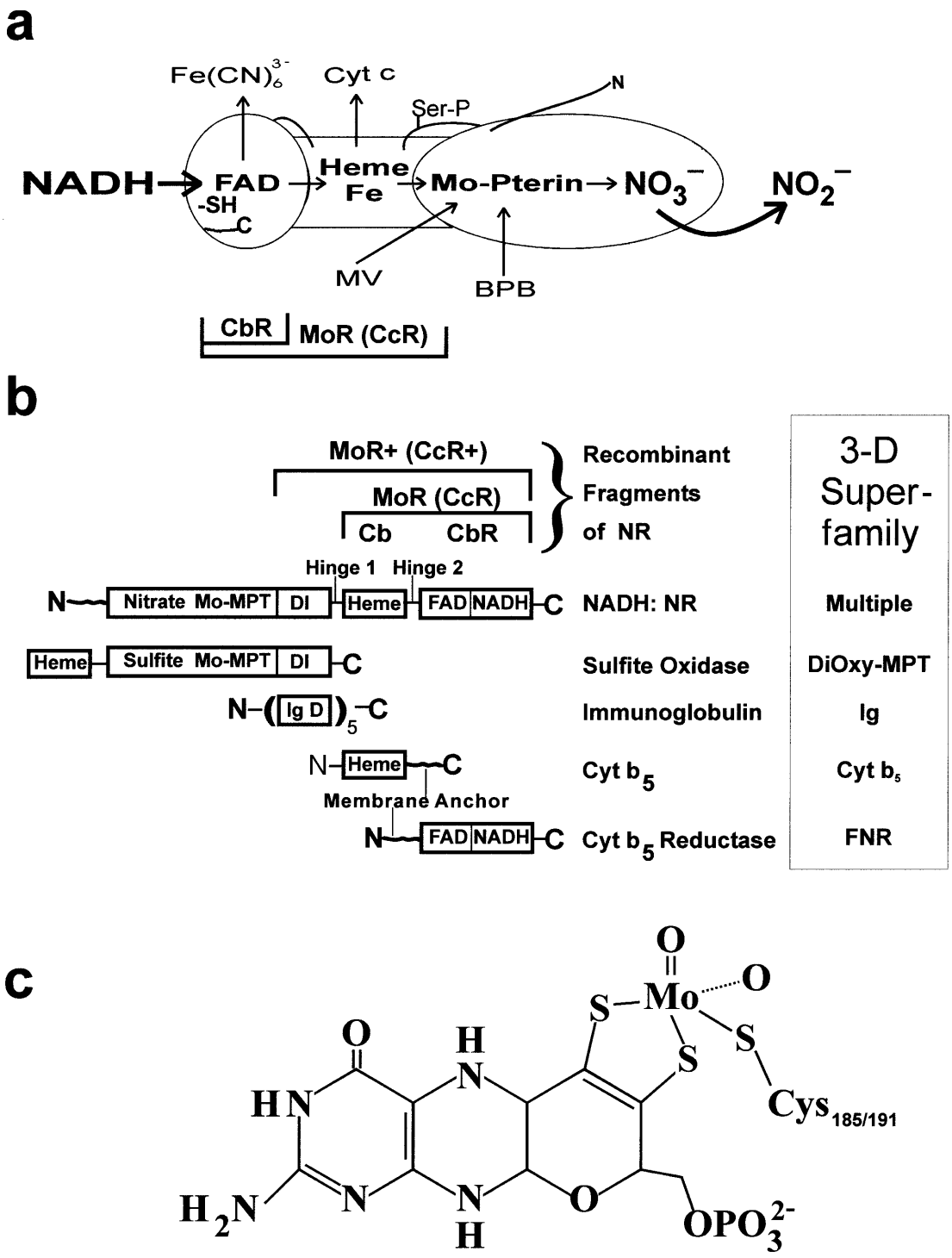

Figure 1. Models of eukaryotic nitrate reductase and the Mo-molybdopterin (Mo-MPT) cofactor. (*a*) Functional schematic for NR showing the complete and partial reactions catalyzed by the enzyme superimposed on a simplified structural model showing the involvement of the FAD, heme-Fe and Mo-MPT in catalysis. The regulatory Ser residue in Hinge 1, which is phosphorylated in light/dark reversible regulation of enzyme activity in plants, is shown, as well as the Cys thiol involved in positioning NADH for efficient electron transfer to the FAD [1]. The relative position of the N-terminus is shown. The functionality of the known recombinant fragments of NR with catalytic activity are shown. Abbreviations: MV, reduced methly viologen; BPB, reduced bromphenol blue. (*b*) Structural schematic for NR and its recombinant fragments with the 3-D superfamilies for the NR domains identified via related proteins and enzymes of known 3-D structure. In NR and SOX [1, 9], DI stands for the dimer interface domain, and in the immunoglobulin, the structurally similar domain is designated Ig D. The designations for the 3-D superfamilies were obtained from the Protein Database. Abbreviation: FNR, ferredoxin $NADP^+$ reductase. (*c*) Structure of the Mo-molybdopterin cofactor based on the 3-D structure of sulfite oxidase, which is identified in the Protein Database as SOX1 [9]. NR has been shown to have a similar coordination sphere for Mo to that found in SOX [16, 17]. The Cys residue is identified by its sequence position in chicken liver SOX (Cys-185) and AtNR2 (Cys-191).

tron transfer may be rate limiting for enzyme activity. Stopped-flow rapid-scanning transient kinetics and other rapid kinetic methods are currently being employed to investigate the rate-limiting processes in NR and establish the catalytic mechanism of the enzyme [3]. Expression of recombinant holo-NR in an active form and the generation of site-directed mutants are also contributing toward gaining understanding of the enzyme's catalytic mechanism [1].

Eukaryotic NR has only limited similarity to prokaryotic nitrate reductase, which also contains Mo and a pterin cofactor, and differs from eukaryotic MPT in having an additional nucleotide; in some cases, two pterins are coordinated to the Mo (see other papers in this issue for more details on bacterial nitrate reductase forms). The bacterial enzymes are either membrane-bound terminal electron acceptors in energy-coupled electron transport/proton-pumping systems or may be soluble enzymes in te periplasmic space involved in denitrification. A 3-D structure has been determined for the nitrate reductase from *Desulfovibrio* which is called NAP [4]. NAP is similar in structure to *Escherichia coli* formate dehydrogenase and has little, if any, sequence similarity to NR, which indicates their conformations and structural families are different [4]. NAP and some other prokaryotic nitrate reductases have an iron-sulfur redox canter (Fe_4S_4) built into the same polypeptide with the Mo-molybdopterin cofactor. The Fe_4S_4 redox center serves as mediator of electron transfer in the enzyme from the electron donor and electron reservoir. No eukaryotic NR has been found to have an iron-sulfur center as a component of its electron transport chain. It has been suggested that NAP has an arginine residue involved with binding nitrate in the active site [4]. This is similar to eukaryotic NR forms [1]. Thus, all forms of nitrate reductase may have some common features in their catalytic mechanism of nitrate reduction, but more detailed studies are needed to firmly establish the mechanisms. NAP has a $k_{cat} = 30\ s^{-1}$, which is significantly slower than eukaryotic NR, with a $k_{cat} = 200–300\ s^{-1}$ [1, 4]. This suggests that the larger, more complex enzyme found in eukaryotic NR with the more compact Mo-MPT may be more catalytically efficient than prokaryotic forms.

Structure of eukaryotic NR

The structure of the NR monomeric unit, which is generally assumed to be catalytically independent of the other subunit in the enzyme complex, is built from modular sections of the polypeptide folded into quasi-independent conformations to house the redox cofactors and form the two active sites as well as the dimer interface region (fig. 1b). This general picture of NR structure is based on a wide body of biochemical evidence, including sequence comparison with other enzymes and proteins, and the recombinant expression of the fragments of NR [1, 5, 6]. Whereas the structure of some NR fragments have been determined and others modeled [1, 2, 7, 8], the 3-D structure of NR has not yet been determined since no one has been able to crystallize holo-NR. However, a 3-D model of holo-NR was generated based on the 3-D structure of mammalian sulfite oxidase (SOX; EC 1.8.2.1) and a model of the Mo reductase fragment of NR (MoR; formerly called the cyt *c* reductase fragment). SOX is a homodimer with three domains [9]: one for binding Mo-MPT and formation of the active site for oxidizing sulfite, one for binding heme-Fe as a Cyt *b* similar in structure to the Cyt *b* in NR, where Cyt *c* is reduced, and one for interfacing between the monomeric units of the enzyme. NR and SOX have been found to have very similar dioxy-Mo-MPT cofactors [1, 9], which suggests that the 3-D structure of SOX Mo-MPT is an excellent model for NR's Mo-MPT (fig. 1c). Whereas the dimeric form of SOX is required for activity like NR [9], the physical attachment of the Cyt *b* in the same polypeptide in not since a plant SOX has been cloned with only the Mo-MPT and dimer interface domains represented in the sequence (see GenBank accession number AF200972). Since NR has about 50% similarity in amino acid sequence with SOX, an atom-replacement model of the core dimeric structure of NR was generated, and two MoR fragments were docked via the similarity in the sequences of the Cyt *b* domains [1]. While the 3-D model of NR has some limitations [1], it serves to establish for the first time the general overall shape of NR and provides some useful information on the potential ligands involved in nitrate binding at the nitrate reducing active site, which have recently been investigated by site-directed mutagenesis. Overall, the monomer of NR can now be viewed as having eight distinct sequence regions (fig. 1b):

(i) an N-terminal sequence which is variable in length for different NR forms and may be involved in activity regulation in plant NR forms; (ii) a Mo-MPT domain with nitrate binding and reducing active site; (iii) dimer interface domain, which also contributes to the nitrate-reducing active site; (iv) Hinge 1 with a variable sequence, a highly sensitive proteolytic site and the site of the regulatory Ser residue in plant NR which becomes phosphorylated; (v) a Cyt *b* domain where heme-Fe is bound; (vi) Hinge 2 which is variable in length and contains a proteolytic site in many NR forms; (vii) a FAD binding domain, which contributes along with the pyridine nucleotide binding domain to form the NAD(P)H reaction active site where the enzyme is reduced, and (viii) an NAD(P)H binding domain at the C-terminus which is joined to the FAD domain by a short linker containing a three-strand β sheet.

The major fragments of NR expressed by recombinant DNA methods are the Cyt *b* reductase fragment (CbR) composed of the two C-terminal domains, for which an X-ray 3-D structure has been determined [7], and the MoR fragment where the Cyt *b* domain is joined to CbR via Hinge 2, for which a 3-D model was generated [9]. The Cyt *b* domain has been expressed in several forms, and a 3-D model generated by comparison to mammalian Cyt b_5 [6, 10]. Although a nitrate-reducing fragment of NR containing the Mo-MPT, interface and Cyt *b* domains was generated by proteolysis of holo-NR [6], no similar fragment has been recombinantly expressed, which is a major challenge to be achieved in future research.

Recombinant expression of holo-NR

Holo-NR has been recombinantly expressed from a number of sources and in different expression systems with varying degrees of success in producing an active nitrate-reducing form of the enzyme (table 1). The most detailed studies have been done with recombinant holo-NR forms expressed in *Pichia pastoris*, a methylotrophic yeast. In collaboration with Crawford [11], we characterized *Arabidopsis* Nia2 (AtNR2) expressed in *Pichia* and generated a nitrate-reducing active site mutant by replacing the essential Cys of the Mo-MPT domain with Ser. This residue is Cys-191 in AtNR2, which corresponds to only one of two invariant Cys residues in NR [1]. The other invariant Cys is found in the CbR fragment of NR, which we had previously mutated to Ser, with this mutant resulting in an enzyme with very low efficiency for electron transfer from NADH to the enzyme's bound FAD [12, 13]. Thus, roles for the invariant Cys residues in NR have been established: Cys-191 in AtNR2 is a required ligand to Mo in the nitrate-reducing active site, whereas Cys-891 of AtNR2 is in the enzyme's other active site where NADH reduces FAD and appears to be critical for positioning the NADH for efficient electron transfer [1]. *Pichia*-expressed AtNR2 has also been altered by site-directed mutagenesis in the Hinge 1 region for studies of the regulation of NR activity by the binding protein known as 14-3-3 [14]. Most recently, we have analyzed the roles of Arg residues in the nitrate-reducing active site by mutating them to Gln in a chimeric form of NR which was expressed in *Pichia*. The Arg residues, Arg-144 and Arg-196 in AtNR2, were identified by comparative sequence analysis of all NR forms and found to be invariant. These Arg residues correspond to active site Arg residues in SOX [9, 15] and have been modeled in the NR active site [1]. When Arg-144 was mutated to Gln, the mutant R196Q enzyme was found to contain virtually no Mo and MPT, which indicated the mutant protein could not form stable complexes with Mo-MPT. The mutation of Arg-196 to Gln resulted in an enzyme form with a high nitrate K_m compared with wild-type enzyme and decreased catalytic efficiency by a factor of 3200. These results differed from a site-directed mutagenesis study of the SOX Arg residue corresponding to ATNR2 Arg-144, which found that it could be replaced by Gln without loss of Mo-MPT binding [15]. Overall, the differences between the roles of these conserved Arg residues in NR and SOX indicate that there is probably significant conformational variation between the active sites in the two enzymes.

Recombinant AtNR2 was analyzed by X-ray absorption spectroscopy and found to have a conformational shift of one of the sulfur ligands coordinated to the Mo center in going from resting to turnover enzyme forms [16]. After reduction with dithionite and reoxidation by nitrate, the arrangement of ligands around the Mo were like those in SOX [17], which are composed of two S from MPT, one S from a Cys residue, and two oxo-ligands [9]. When nitrite and nitrate were removed from NR, it returned to the resting conformation which is not found in SOX [16]. NR appears to have a startup process during its first reduction, after which it probably remains in the active form. These results emphasize a difference between NR and SOX in their respective

Table 1. Recombinant expression of holo-nitrate reductase in *Pichia pastoris* and other organisms [1, 3, 11–14 and unpublished data of various research groups].

NR form	cDNA source	Expression system	NR purified	Mutants	Biochemical analysis
NADH:NR	*Arabidopsis nia*2 (AtNR2)	*Pichia*	yes	yes	detailed
NADH:NR Chimeria	Zmnr1/AtNR2	*Pichia*	yes	no	some
NADH:NR	spinach	*Pichia*	paratially	no	not yet
NADH:NR	tobacco	*Pichia*	partially	no	not yet
NADH:NR	AtNR2	*E. coli*	inactive	no	antibody prepared
NADH:NR	tobacco	*Saccharomyces*	inactive	no	some
NADH:NR	various plants	tobacco/*Arabidopsis*	no	many	some
NADPH:NR	*Aspergillus nidulans*	*A. nidulans* NR^- strain	no	yes	some
NADPH:NR	*Neurospora crassa*	*N. crassa* NR^- strain	no	yes	some

Table 2. Recombinant fragments of NR expressed in *Escherichia coli* and *Pichia pastoris*. NR sources of the expressed enzyme fragments and some biochemical properties are summarized [1, 2, 6, 12, 18–22].

NR fragment	cDNA source/expression system	Cofactors	Active site	Protein M_r (kDa)	3-D structure	Steady-state kinetics	Transient kinetics	Redox potential
CbR	Zmnr1/*E. coli*	FAD	NADH	30	X-ray	partial	yes	yes
CbR	spinach/*E. coli*	FAD	NADH	30	model	partial	no	no
CbR	*Neurospora crassa*/*E. coli*	FAD	NADPH	30	model	detailed	no	no
CbR	spinach/*E. coli*	FAD	NADH	30	none	detailed	no	yes
Cb	*Chlorella*/*E. coli*	heme-Fe	none	12 and 35	models	–	–	yes
MoR (CcR)	Zmnr1S/*E. coli*	FAD heme-Fe	NADH	58	model	partial	no	no
MoR (CcR)	Zmnr1/*Pichia*	FAD, heme-Fe	NADH	42	model	detailed	yes	yes
Mor (CcR)	spinach/*Pichia*	FAD, heme-Fe	NADH	42	model	detailed	yes	yes
CbR-Cb_5	spinach and Rat/*E. coli*	FAD, heme-Fe	NADH	43	none	detailed	no	no
MoR + (CcR +)	Zmnr1/*Pichia*	FAD heme-Fe	NADH	67	model	detailed	no	yes

Mo-containing active sites. While much more study is needed to define the active sites of NR and SOX, caution is warranted in concluding that these enzymes are highly similar in active site conformation. Thus, it is clear that recombinant expression of active NR in *Pichia* will contribute significantly to gaining understanding of the biochemistry of NR.

Recombinant fragments of NR

As mentioned above, various fragments of NR have been expressed in *E. coli* and *Pichia* (table 2). The study of the NR fragments has contributed significantly to our understanding of NR biochemistry, especially with respect to the functionality of the FAD domain of the enzyme and the residues responsible for determining pyridine nucleotide specificity [1, 2, 7, 8, 12, 13, 18–21]. The 3-D structure of the CbR fragment of corn NR expressed in *E. coli* demonstrated that this portion of NR is structurally related to ferredoxin-$NADP^+$ reductase and the family of enzymes known as the FNR type of flavin dehydrogenases [1, 2, 7, 8]. The role of the proposed NR dimer interface domain was investigated by expressing the MoR fragment of corn NADH:NR with Hinge 1 and the putative interface domain attached, which resulted in dimerization of MoR [18]. Thus, the dimer interface domain is an independently folded and stable region of NR serving the role predicted for it [1], based on its role in SOX [9]. Directed mutagenesis showed that the CbR from *Neurospora crassa* NADPH:NR could be converted to an NADH-dependent enzyme by replacing a single Ser with an Asp in the NADPH domain [19]. The spinach MoR expressed in *Pichia* was used for a pre-steady-state kinetic analysis of electron transfer from NADH to the FAD and heme-Fe in the Cyt *b* domain, which complemented previous studies done on the CbR fragment [12, 13, 20]. Further kinetic analyses of the MoR fragment of corn NR have clarified the electron transfer rates from NADH to the heme-Fe in the Cyt *b* domain via the FAD and resulted in kinetic schemes for these electron transfer processes [18]. Finally, the expression of MoR fragments with and without the regulatory Ser in Hinge 1 helped in the identification of the exact residue phosphorylated in NR [21]. Recombinant expression of NR fragments is expected to continue to add to our understanding of NR biochemistry since these fragments are simpler than the complete enzyme, which makes experimental analysis easier to do and interpret.

Toward understanding the catalytic mechanism of NR

The long-standing explanation of electron transport as the rate-limiting process in NR catalysis [1, 6] still

Table 3. Standard redox potentials of NR cofactor couples for holo-NR and its fragments.

Redox couple	AtNR2	Spinach NR	Chlorella NR		Corn MoR+	Corn MoR	Spinach MoR	Corn CbR		Spinach CbR		Chlorella Cb
	WT, N-T and CbR*							WT	C242S	WT	C240S	35 kDa 10 kDa†
Temperature	22 °C (80 K for Mo)	25 °C	25 °C	173 K	22 °C	22 °C	25 °C	25 °C	25 °C	25 °C	25 °C	25 °C
Mo^{VI}/Mo^{V}	+40	+2	+15	−34								
Mo^{V}/Mo^{IV}	−30	−6	−25	−54								
Mo^{VI}/Mo^{IV}	+5	−2	−5	−44								
Heme-Fe^{3+}/Fe^{2+}	−40	−123	−160	(−166 N-T)*	−60	+20	+15					−28, +16
$FAD/FAD^{\bullet-}$		−380	−372									
$FAD^{\bullet-}/FADH_2$		−180	−172		−170	−150	−170					
$FAD/FADH_2$	−270	−280	−272	(−286 CbR)*	−230	−260	−250	−287	−279	−270	−219	
$FAD/FADH_2+NAD^+$							−210	−265	−268	−190	−191	

* Two fragments of Chlorella NR generated by proteolytic nicking were analyzed: N-T, Heme-Fe/Mo-MPT fragment; and CbR, flavin containing 30-kDa fragment.
† Two recombinant forms of the Cb fragment of Chlorella have been expressed: 35-kDa fragment, Cb-Hinge 1 interface domain; 10 kDa, Cb alone.
Midpoint redox potentials are shown in mV versus stadard hydrogen electrode at pH 7. There is an estimated error of ±10 mV. These data are from a number of different studies, including some previously unpublished results on AtNR2 [1, 6, 13, 18, 20, 22]. Abbreviations: WT, wild type; C242S/C240S, CbR mutants with invariant Cys replaced with Ser. For definition of the structure and functionality of CbR, Cb, MoR and MoR+, see fig. 1A and B.

appears to be valid, but there is a lack of data on the actual internal electron transfer rates in holo-enzyme. One place to begin with the description of the catalytic mechanism of nitrate reductase is with an evaluation of the redox potentials of the enzyme's cofactors. A variety of methods with different holo-NR and fragments have been used to determine redox potentials for the three prosthetic groups in NR and its fragments; however, the results from these analyses agree well (table 3). Voltammetric methods have recently provided new insight into the impact on the redox potentials due to interactions of FAD with NAD^+ and between the Cyt *b* domain and the N-terminal portion of NR [18, 22]. Ratnam et al. [13] were the first to show that the binding of NAD^+ to the CbR fragment of corn NR shifted the redox potential of the FAD less negative. Subsequently, redox analysis of CbR and MoR fragments of NR showed that the presence of half-saturating or higher concentrations of NAD^+ or related pyridine nucleotide analogues lowered the redox potetial of FAD by as much as 40–80 mV [18, 22]. Although this effect of NAD^+ on the FAD has not been shown with the holo-NR (table 3), it appears clear that the binding of the oxidized pyridine nucleotide to FAD in a charge-transfer complex [1, 2, 6, 13, 20] brings its redox potential closer to the Cyt *b* in the enzyme. On the other hand, the redox potential of heme-Fe is shifted to a more negative potential by the N-terminal portion of NR, as shown by the analysis of the enzyme's fragments as compared with holo-NR. This was first observed when the redox potential was determined for two recombinant forms of the Cyt *b* of *Chlorella* NR: one with a large N-terminal extension and one with only the Cyt *b* domain [6]. The 'free' Cyt *b* has a potential similar Cyt b_5 at about +15 mV [1, 6], which is the same when MoR is analyzed, showing that the addition of the CbR fragments at the C-terminus has no influence on the Cyt *b*'s redox potential [18, 20]. However, in the larger Cyt *b* fragment expressed from the *Chlorella* NR complementary DNA (cDNA) and in the MoR fragment with Hinge 1 and the interface domain attached at the N-terminus (called MoR+), the Cyt *b* redox potential is shifted more negative and approaches the more negative values reported for the heme-Fe in holo-NR from several sources [1, 18]. In holo-NR, the reduction by NADH leads to a charge-transfer complex between NAD^+ and $FADH_2$, which breaks down very slowly [20], and this complex is probably involved with reduction of the heme-Fe for the first step in internal electron transfer. To summarize the redox potentials: FAD is poised at −280 to −250 mV and shifted to −210 to −190 mV with NAD^+ bound; heme-Fe is poised at +15 to +20 mV in the free form and shifts to −60 to −30 with a partial N-terminal sequence and in holo-NR to −160 to −120 mV; and Mo is poised

Reduction State	NR^0	NR^{1-}	NR^{2-}	NR^{3-}	NR^{4-}	NR^{5-}
Number of Microstates	1	3	5	5	3	1
Microstates	S_1 Mo^{VI} heme-Fe^{3+} FAD	S_2 Mo^{V}	S_5 Mo^{IV}	S_{10} Mo^{IV} heme-Fe^{2+}		
		S_3 heme-Fe^{2+}	S_6 Mo^{V} heme-Fe^{2+}	S_{11} Mo^{IV} $FAD\bullet^-$	S_{15} Mo^{IV} heme-Fe^{2+} $FAD\bullet^-$	
		S_4 $FAD\bullet^-$	S_7 Mo^{V} $FAD\bullet^-$	S_{12} Mo^{V} $FADH_2$	S_{16} Mo^{IV} $FADH_2$	S_{18} Mo^{IV} heme-Fe^{2+} $FADH_2$
			S_8 heme-Fe^{2+} $FAD\bullet^-$	S_{13} Mo^{V} heme-Fe^{2} $FAD\bullet^-$	S_{17} Mo^{V} heme-Fe^{2+} $FADH_2$	
			S_9 $FADH_2$	S_{14} heme-Fe^{2+} $FADH_2$		

Figure 2. Redox microstates of the FAD, heme-Fe and Mo-MPT cofactors in oxidized and reduced NR. Only the reduced species in each microstate are shown except for fully oxidized NR. This diagram is similar to one representing the reduction states for xanthine oxidase [23]. Below each NR reduction state symbol is the number of microstates of the enzyme. For each reduction state of NR, the microstates are numbered sequentially, beginning with the lowest energy state. The flavin semiquinone is shown as the anionic form since this is the type observed in NR [3].

near 0 mV in holo-NR. Thus, it is clear that electrons would flow toward the Mo center when the enzyme is reduced by NADH. This achieves two effects—the two electrons needed for reduction of nitrate to nitrite are thermodynamically driven to the Mo, and at the same time the FAD is left oxidized and ready to accept another two electrons from NADH. Although some equilibration of the electrons within NR is expected, the large difference between the redox potentials to Mo couples and the heme-Fe couple indicated most of the electrons will reside in the Mo center at equilibrium. Consequently, since NR is a two active site enzyme, the FAD may be reduced by NADH even before the reduced Mo transfers its electrons to nitrate.

Analysis of the distribution of electrons in oxidized and reduced enzyme forms was previously done for xanthine oxidase/xanthine dehydrogenase, which is slightly more complex than NR, since it contains four redox groups, namely Mo-MPT with terminal S, FeS-I, and FeS-II and FAD, resulting in 36 microstates for the enzyme [23]. A similar analysis for NR shows that is has 18 microstates for the oxidized and all possible reduced forms (fig. 2). NR can accept a total of five electrons: two in FAD, one in heme-Fe and two in Mo, which has been shown by electron titration of several NR forms [1, 6]. Since NADH is a two-electron reductant, the major reduced forms of the enzyme are NR^{2-} and NR^{4-} (assuming the resting enzyme is NR^0). However, in the absence of an electron acceptor, two 2-electron-reduced enzyme molecules will react to produce NR^{1-} and NR^{3-}, which would lead to NR^{3-} and NR^{5-} when further reduced by NADH. In addition, two 4-electron-reduced NR molecules will react to produce NR^{3-} and NR^{5-}, or two- and four-electron-reduced enzymes will react to produce NR^{1-} and NR^{5-}. Although intermolecular reactions of various reduced

forms of NR with one another are expected to be rather slow compared with rates of reduction of NADH, it seems possible that intramolecular electron transfers may occur between monomer subunits in NR dimer and tetramer forms, which may be much faster. In other words, all possible microstats of NR may occur in in vitro experiments, especially when the enzyme is reduced in the absence of electron acceptors under anaerobic conditions. While this may seem not too important considering the expected alternation of NR between two-electron-reduced and fully oxidized forms during normal turnover with nitrate, the fully reduced or five-electron-reduced NR is an interesting form to study in evaluating the mechanism of the enzyme. For example, the rate at which fully reduced NR reacts with nitrate is expected to be greater than the turnover rate under standard conditions with both NADH and nitrate present, if the rate of electron transfer is the rate-limiting process in NR catalysis. This hypothesis was recently tested by reacting fully reduced AtNR2 with nitrate and NADH under anaerobic conditions at 5 °C in a freeze-quench apparatus where acid was used to stop the reaction instead of freezing [3, and W. H. Campbell and D. J. Lowe, unpublished results]. The rate of nitrite formation was about four times greater during the first 5 ms of this reaction than the turnover rate at this temperature. This approach has not yet been fully exploited, but it is clear that it will be useful for establishing the maximum nitrate reduction rate catalyzed by NR in the absence of electron transfer.

The rate-limiting process in NR catalysis

A variety of experiments have been used to suggest that the rate-limiting process in NR catalysis is internal electron transfer [1, 6]. This contrasts sharply with some related Mo-containing enzymes like xanthine oxidase and SOX where the initial reduction of the enzyme is rate limiting under most circumstances and internal electron transfer is very rapid [23–25]. For these two enzymes, substrate reduces the Mo center first. Thus, it might be predicted that in NR the rate-limiting process might be nitrate reduction at the Mo center. The steady-state catalytic efficiency of the two active sites of NR illustrates this point, where NADH reduction of *Chlorella* NADH:NR has a $k_{cat}/K_M = \sim 70\ \mu M^{-1}\ s^{-1}$, and nitrate reduction by NR has a $k_{cat}/K_M = 1–3\ \mu M^{-1}\ s^{-1}$ at 25 °C, depending on the ionic strength [26]. Thus, reduction of NR by NADH is 20–70 times more efficient than reduction of nitrate by the reduced enzyme. However, when reduced MV is used as the electron donor, the efficiency of nitrate reduction of *Chlorella* NAH:NR improved to $2–10\ \mu M^{-1}\ s^{-1}$ at 25 °C, depending on the ionic strength [26]. Since it now appears clear that MV donates electrons directly to the Mo-MPT center in NR, bypassing the FAD and heme-Fe centers, this two- to threefold improvement in catalytic efficiency for nitrate reduction probably reflects the actual rate for nitrate being reduced by Mo^{IV} in the enzyme. As described in the previous section of this review, we have recently been able to directly demonstrate the greater efficiency of nitrate reduction by fully reduced AtNR2 in a rapid-mixing acid quench experiment as compared to steady-state turnover under the similar conditions [3]. Overall, it appears that the internal electron transfer rate of NR is from two to three times slower than the rate of nitrate reduction at the Mo active site.

To begin a more quantitative approach to demonstrating that internal electron transfer is rate limiting in NR catalysis, a series of catalytic rate constant models have been developed by NR, using NADH as the pyridine nucleotide electron donor (fig. 3). With these models and rapid-reaction kinetic methods, it is expected that rate constants for each step in NR catalysis will be defined. The simplified catalytic cycle models begin by defining rate constants for the two half reactions catalyzed by NR, which are designed k_2 and k_4^* (fig. 3A). This numbering is used since the rate constants for formation of the Michaelis complexes with the substrates should be designated k_1 and k_3, for binding of NADH and nitrate to their respective active sites. But these preliminary steps in catalysis are expected to be much faster than overall catalysis and are ignored here to simplify the models. These rate constants k_2 and k_4^* are second order and equal to the catalytic efficiencies for the enzyme's active sites, which were discussed above. So the rate constants k_2 and k_4^* are ~ 70 and $1–3\ \mu M^{-1}\ s^{-1}$. It should be recognized readily that k_4^* is determined by either the electron transfer rate or the rate of nitrate reduction by Mo, depending on which process is slower. Thus, a simple refinement is used next to break out the rate of internal electron transfer, which also begins to include the definition of the microstates of NR imvolved in the catalytic steps (fig. 3B). Here, rate constant k_2 is the same as in the simpler model, and k_4 is equal to the catalytic efficiency of reduced MV nitrate reduction, which is $2–10\ \mu M^{-1}\ s^{-1}$, or perhaps greater. The rate constant for internal electron transfer, k_{ET}, is first order and difficult to derive from steady-state kinetic analysis. In addition, internal electron transfer is composed of four 1-electron transfer steps, as illustrated in the last model (fig. 3C). Here the electron transfer rate constants between the microstates of NR identified for the two-electron-reduced enzyme are presented, and it is clear that one of these steps would be the slowest and determine the overall internal electron transfer rate, k_{ET}, if this process is rate limiting in NR catalysis. In order words, the rate of internal electron

A. Simplified catalytic mechanism with reductive and oxidative half-reactions:

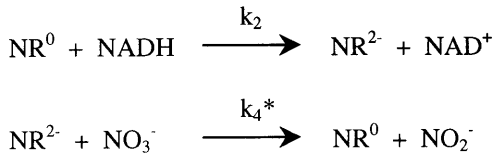

B. Simplified catalytic mechanism with one step internal electron transfer (rate constant = k_{ET}):

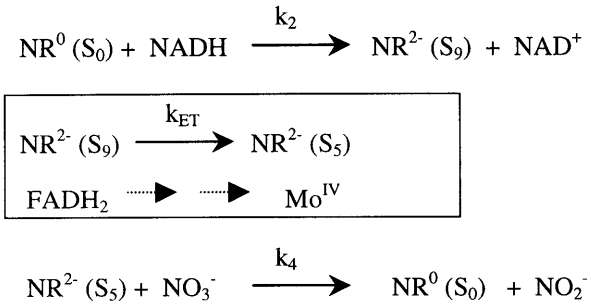

C. Simplified catalytic mechanism with individual one-electron internal electron transfer steps:

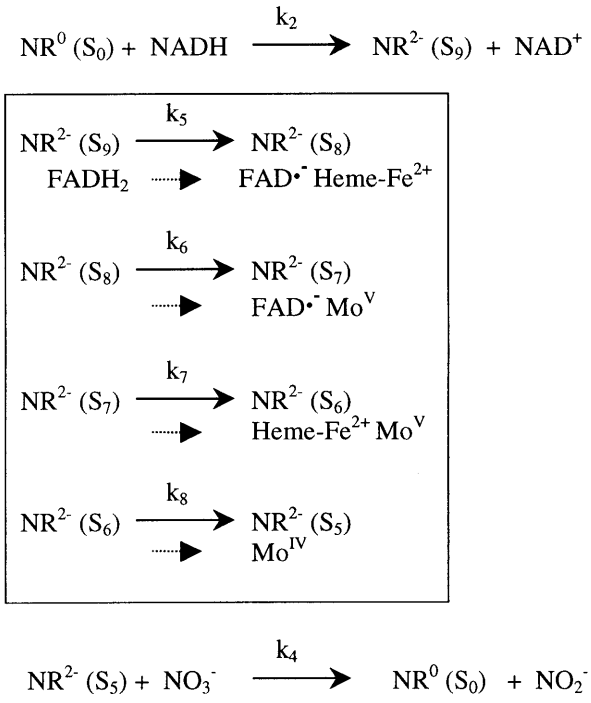

Figure 3. Simplified NR catalytic cycles for identification of key rate constants in the mechanism of catalysis. The numbering of the rate constants is based on reserving constants k_1 and k_3 for the formation of the Michaelis complexes of NR with NADH and nitrate, respectively. Formation of Michaelis complexes and release of product steps in the mechanism are not shown. Rate constants k_2 and k_4 are second order in these models with units = $M^{-1}\ s^{-1}$, which are for irreversible steps in catalysis. All other rate constants are first order. The rate constant k_{ET} is a composite representing the slowest step(s) in internal electron transfer. When internal electron transfers are shown, the reduction microstate of NR involved in catalysis is identified and the rate equations outlined by a box. The reduced redox cofactors of NR in each microstate of reduction are also shown within the boxed sections to illustrate the progression of the internal electron transfer reactions.

transfer from reduced FAD states to heme-Fe or from reduced heme-Fe to Mo are the key steps to focus on.

Pre-steady-state and steady-state kinetic analysis of CbR and MoR fragments of NR with NADH as electron donor and FeCN and Cyt *c* as electron acceptor are useful for unraveling some of the complexity of internal electron transfer [12, 13, 18, 20]. First, the steady-state catalytic efficiencies of FeCN and Cyt *c* reduction for various MoR forms are 40–200, 80–140 and 220–300 $\mu M^{-1}\ s^{-1}$, for NADH, FeCN and Cyt *c*, respectively [18]. These catalytic steps involve electron transfer from NADH to FAD with a k_{cat} of 2300 to 2700 s^{-1} for FeCN reduction and from reduced FAD forms to heme-Fe with a k_{cat} of 1300–1800 s^{-1} for the Cyt *c* reduction reaction, which indicates that the initial internal electron transfers are faster than NR catalysis by large factors. This indicates that k_5 and k_7 are not likely to be rate limiting in NR (fig. 3C). The pre-steady-state analysis of CbR and MoR demonstrates that the pseudo-first-order reduction of FAD by NADH is extremely fast, with a rate of 500–700 s^{-1} at 10–15 °C and basically limited by the rate of diffusion [13, 18]. This has also been shown with AtNR2, where NADH reduced FAD with a rate of 320 s^{-1} at 15 °C [3]. Electron transfer from $FADH_2$ to heme-Fe is also rapid at 300 s^{-1} for MoR and 420 s^{-1} for AtNR2 [3, 18]. The final electron transfers from reduced heme-Fe to Mo forming Mo^{V} and Mo^{IV} have been observed indirectly by monitoring the rate of oxidation of fully reduced NR by nitrate in stopped-flow rapid-scanning spectrophotometric experiments at 5 and 15 °C [3]. Here, $FADH_2$ and heme-Fe^{2+} were oxidized at rates of 200–300 s^{-1} for AtNR2, which suggests k_6 is rapid in internal electron transfer and greater than overall catalysis. However, these experiments did not provide a clear definition of the final internal electron transfer step, k_8, which appears to most likely represent the rate-limiting process in NR catalysis. In other words, transferring the second electron from heme-Fe^{2+} to Mo^{V} to fully reduce it to Mo^{IV} is likely to be the slowest electron transfer step in NR catalysis. However, since currently available data are preliminary [3], further experimentation is needed to firmly establish this suggestion and define a rate constant for the rate-limiting process in NR catalysis.

Future prospects for advancement of NR biochemistry

Overall, much of the complexity of eukaryotic NR is being unraveled in current research, and it can be expected that the structure and function of this enzyme family will be clearly understood in the near future. This is especially important since NR has become useful in environmental cleanup of nitrate pollution, which is a problem worldwide [1]. NR is already being used in nitrate detection kits, and a nitrate biosensor based on NR is being developed. Enzymatic nitrate removal processes involving NR have been studied and may offer an efficient method for purification of nitrate-polluted drinking water at the point of use. This practical side of NR biochemistry and biotechnology proves the value of the large investment in basic research on NR made by the public over the past 50 years.

Acknowledgments. The U.S. National Science Foundation, the U.S. Department of Agriculture, and the State of Michigan Research Excellence Fund are thanked for grants which have supported the research carried out in the author's laboratories over the past 25 years. I thank Prof. David J. Lowe for helpful discussions on the catalytic mechanism of NR.

1 Campbell W. H. (1999) Nitrate reductase structure, function and regulation: bringing the gap between biochemistry and physiology. Annu. Rev. Plant Physiol. Plant Mol. Biol. **50:** 277–303
2 Campbell W. H. (1996) Nitrate reductase biochemistry comes of age. Plant Physiol. **111:** 355–361
3 Mertens J. A., Campbell W. H., Skipper L. and Lowe D. J. (1999) Electron transfer from FAD to heme-Fe in plant NADH:nitrate reductase. In: Flavins and Flavoproteins, pp. 131–134. Ghislat S., Kroneck P., Macheroux P. and Sund H. (eds), Agency for Scientific Publications, Berlin
4 Dias J. M., Than M., Humm A., Huber R., Bourenkov G., Bartunik H. et al. (1999) Crystal structure of the first dissimilatory nitrate reductase at 1.9 Å solved by MAD methods. Structure **7:** 65–79
5 Campbell W. H. and Kinghorn J. R. (1990) Functional domains of assimilatory nitrate reductases and nitrite reductases. Trends Biochem. Sci. **15:** 315–319
6 Solomonson L. P. and Barber M. J. (1990) Assimilatory nitrate reductase—functional properties and regulation. Annu. Rev. Plant Physiol. Plant Mol. Biol. **41:** 225–253
7 Lu G., Campbell W. H., Schneider G. and Lindqvist Y. (1994) Crystal structure of the FAD-containing fragment of corn nitrate reductase at 2.5 Å resolution: relationship to other flavoprotein reductases. Structure **2:** 809–821
8 Lu G., Lindqvist Y., Schneider G., Dwivedi U. N. and Campbell W. H. (1995) Structural studies on corn nitrate reductase. Refined structure of the cytochrome b reductase fragment at 2.5 Å, its ADP complex and an active site mutant and modeling of the cytochrome b domain. J. Mol. Biol. **248:** 931–948
9 Kisker C., Schinedelin H., Pacheco A., Wehbi W. A., Garrett R. M., Rajagopalan K. V. et al. (1997) Molecular basis of sulfite oxidase deficiency from the structure of sulfite oxidase. Cell **91:** 973–983
10 Meyer C., Levin J. M., Roussel J.-M. and Rouze P. (1991) Mutational and structural analysis of the nitrate reductase heme domain of *Nicotiana plumbaginifolia*. J. Biol. Chem. **266:** 20561–20566
11 Su W., Mertens J. A., Kanamaru K., Campbell W. H. and Crawford N. M. (1997) Analysis of wild-type and mutant plant nitrate reductase expressed in the methylotrophic yeast *Pichia pastoris*. Plant Physiol. **115:** 1135–1143
12 Dwivedi U. N., Shiraishi N. and Campbell W. H. (1994) Identification of an 'essential' cysteine of nitrate reductase via mutagenesis of its recombinant cytochrome b reductase domain. J. Biol. Chem. **269:** 13785–13791
13 Ratnam K., Shiraishi N., Campbell W. H. and Hille R. (1995) Spectroscopic and kinetic characterization of the recombinant wild-type and C242S mutant of the cytochrome b reductase fragment of nitrate reductase. J. Biol. Chem. **270:** 24067–24072

14 Kanamaru K., Wang R., Su W. and Crawford N. M. (1999) Ser-534 in the hinge 1 region of *Arabidopsis* nitrate reductase is conditionally required for binding of 14-3-3 proteins and in vitro inhibition. J. Biol. Chem. **274:** 4160–4165
15 Garrett R. M., Johnson J. L., Graf T. N., Feigenbaum A. and Rajagopalan K. V. (1998) Human sulfite oxidase R160Q: identification of the mutation in a sulfite oxidase-deficient patient and expression and characterization of the mutant enzyme. Proc. Natl. Acad. Sci. USA **95:** 6394–6398
16 George G. N., Mertens J. A. and Campbell W. H. (1999) Structural changes induced by catalytic-turnover at the molybdenum site of *Arabidopsis* nitrate reductase. J. Am. Chem. Soc. **121:** 9730–9731
17 George G. N., Garrett R. M., Prince R. C. and Rajagopalan K. V. (1996) XAS and EPR spectroscopic studies of site-directed mutants of sulfite oxidase. J. Am. Chem. Soc. **118:** 8588–8592
18 Mertens J. A., Shiraishi N. and Campbell W. H. (2000) Recombinant expression of molybdenum reductase fragments of plant nitrate reductase at high levels in *Pichia pastoris*. Planta Physiol. **23:** 743–756
19 Shiraishi N., Croy C., Kaur J. and Campbell W. H. (1998) Engineering of pyridine nucleotide specificity of nitrate reductase: mutagenesis of recombinant cytochrome b reductase fragment of *Neurospora crassa* NADPH:nitrate reductase. Arch. Biochem. Biophys. **355:** 104–115
20 Ratnam K., Shiraishi N., Campbell W. H. and Hille R. (1997) Spectroscopic and kinetic characterization of the recombinant cytochrome c reductase fragment of nitrate reductase: identification of the rate limiting catalytic step. J. Biol. Chem. **272:** 2122–2128
21 Bachmann M., Shiraishi N., Campbell W. H., Yoo B.-C., Harmon A. C. and Huber S. C. (1996) Identification of the major regulatory site as Ser-543 in spinach leaf nitrate reductase and its phosphorylation by Ca^{2+}-dependent protein kinase in virto. Plant Cell **8:** 505–517
22 Barber M. J., Trimboli A. J., Nomikos S. and Smith E. T. (1997) Direct electrochemistry of the flavin domain of assimilatory nitrate reductase. Arch. Biochem. Biophys. **345:** 88–96
23 Olson J., Ballou D. P., Palmer G. and Massey V. (1974) The mechanism of action of xanthine oxidase. J. Biol. Chem. **249:** 4363–4382
24 Hille R. (1996) The mononuclear molybdenum enzymes. Chem. Rev. **96:** 2757–2816
25 Pacheco A., Hazzard J. T., Tollin G. and Enemark J. H. (1996) The pH dependence of intramolecular electron transfer rates in sulfite oxidase at high and low anion concentrations. J. Biol. Inorg. Chem. **4:** 390–401
26 Trimboli A. J. and Barber M. J. (1994) Assimilatory nitrate reductase: reduction and inhibition by $NADH/NAD^+$ analogs. Arch. Biochem. Biophys. **315:** 48–53